A Testbed and Simulation Framework for Air-based Molecular Communication using Fluorescein

Sunasheer Bhattacharjee
Kiel University, Germany
sub@tf.uni-kiel.de

Martin Damrath
Kiel University, Germany
md@tf.uni-kiel.de

Fabian Bronner
Paderborn University, Germany
fabian.bronner@ccs-labs.org

Lukas Stratmann
TU Berlin, Germany
stratmann@ccs-labs.org

Jan Peter Drees
University of Wuppertal, Germany
jan.drees@uni-wuppertal.de

Falko Dressler
TU Berlin, Germany
dressler@ccs-labs.org

Peter A. Hoeher
Kiel University, Germany
ph@tf.uni-kiel.de

ABSTRACT

Molecular communication can enable transmission of information within industrial networks comprising of pipes, ducts, etc. This work emulates the system by introducing an air-based macroscopic molecular communication testbed, exploiting the fluorescence property of a water-based solution of an organic compound called fluorescein. An efficient transmitter in the form of an industrial sprayer, coupled with a high-speed camera-based detection, eventually paves way to achieve higher data transmission rates. The transmission distances considered are in the range of several centimeters to meters. Additionally, models for spray nozzle injector and camera receiver are described to simulate the testbed in a particle-based simulator. These simulated models are calibrated to the used transmitter and receiver and are compared with the analytical models obtained from the testbed measurements.

CCS CONCEPTS

• **Networks** → **Network simulations**; • **Computing methodologies** → *Model development and analysis.*

KEYWORDS

Molecular communication, testbed, fluorescein, optical detection, particle simulation

ACM Reference Format:
Sunasheer Bhattacharjee, Martin Damrath, Fabian Bronner, Lukas Stratmann, Jan Peter Drees, Falko Dressler, and Peter A. Hoeher. 2020. A Testbed and Simulation Framework for Air-based Molecular Communication using Fluorescein. In *The Seventh Annual ACM International Conference on Nanoscale Computing and Communication (NANOCOM '20), September 23–25, 2020, Virtual Event, USA.* ACM, New York, NY, USA, 6 pages. https://doi.org/10.1145/3411295.3411298

NANOCOM '20, September 23–25, 2020, Virtual Event, USA

ACM ISBN 978-1-4503-8083-6/20/09…$15.00
https://doi.org/10.1145/3411295.3411298

1 INTRODUCTION

Molecular communication (MC) has been a topic of interest among the wireless communication research community for a significant period of time now [14] which is being pondered upon to be a part of 6G systems and beyond [10]. It uses molecules as primary information carriers between a transmitter (Tx) and a receiver (Rx) over a given channel. MC has evolved over millions of years, and is used by nature in different forms. Inter- and intra-cellular signaling occurring within the body of a living organism is one such phenomenon [19]. Social insects such as ants also use chemical signals for communication purposes [11]. Inspired by these occurrences, MC can potentially be used at a macro-scale level targeting those industrial applications where deployment of infrastructure for both wired and wireless communications is a challenge. Areas which include monitoring of underwater environments with high concentration of salt, tunnels and pipeline networks for detection of leakages, etc., can effectively exploit the advantages of MC [6]. Prior to the standardization of any industry-oriented system application, communication theory pertaining to MC involving channel impulse response (CIR) analysis, system model design, achieving higher data rates through MC-based modulation schemes, etc. still remain open research topics. Therefore, designing a testbed becomes a crucial starting point to perform preliminary tests and analyses in order to understand the system better, and also to incorporate the aforementioned aspects efficiently. At this stage, simultaneously setting up a simulation environment which emulates the properties of a real-time testbed also proves to be essential. This brings more flexibility to the system in terms of seamless addition/alteration of parameters in order to study the effects on the dynamics governing the entire communication process.

The first testbed concerning air-based macro-scale MC was designed and implemented by Farsad et al. [5], where an electronic sprayer was used as Tx, alcohol was used as the message carrier over the air-based channel, and a metal-oxide sensor was used as Rx. The non-linearities, high inter-symbol interference (ISI) and saturation level attained by the detector were major impediments to the system. Hence, MC alternatives other than alcohol-based detection were explored such as odor-based detection using volatile organic compounds and a mass spectrometer [9]. Transfer of information

using a system of chemical vapor emitter and photoionization detectors under a constant gas flow in an enclosed environment was also introduced by Ozmen et al. [16]. Atthanayake et al. [2] presented the use of fluorescent dye as the information carrier concerning fluid-based MC with a detection process involving particle image velocimetry. Another MC testbed introducing planar laser-induced fluorescence for signal propagation in water-based environment was presented by Abbaszadeh et al. [1]. The channel model, in this case, was based on the detection of the fluorescent dye concentration. The impulse response, however, was much wider in the time-domain, which again would have lowered the data transmission rates with increased ISI.

This work introduces a macroscopic air-based molecular communication testbed incorporating a fluorescence-producing organic compound called fluorescein. Here, a solution of fluorescein in water is sprayed through the air channel. With a high optical detectability, a water-based fluorescein solution produces a distinct emission at approximately 548 nm under the influence of an ultraviolet (UV) light source. Since the air-based channel offers lower resistance compared to a more viscous water-based channel, the data transmission rates are comparatively faster with much lower ISI. The testbed provides a platform for a prospective gamut of real-world analyses which throw light on the effects of air-drag, turbulence, gravitational pull, etc on molecular propagation.

Simulating this testbed in existing simulators for molecular communication faces several issues [3]. Particle-based MC simulators like BiNS2 [7] and AcCoRD [15] as well as analytical simulators like nanoNS3 [12] simulate diffusion and flow for the movement of carrier particles between Tx and Rx. However, in the presented testbed, the injection of the nozzle itself is the main reason for carrier movement. While previous simulators *emit* particles (i.e., release them without adding to their velocity), the simulator needs to *spray* them into the environment. The presented nozzle model is calibrated with data from the real testbed, following a similar approach as Sidahmed et al. [18]. On the Rx side, the aforementioned simulators count the number of particles within a given region or passing a given section. This approach does not take overlaps of the particles into account (droplets in the foreground obscuring other droplets), which affects the Rx video footage. New models for a spray nozzle and a camera Rx are integrated into the *Pogona simulator*, which will be released as open-source software.

The major contributions of the paper include the introduction of the air-based MC testbed mainly focusing on the Tx, Rx, communication channel, and the information carrier as well as two additional modules to allow the simulation of the testbed which include: (i) a spray nozzle injector that creates new particles with an initial velocity and direction for each time step the injector is turned on and (ii) a camera Rx that detects the simulated particles by their reflecting light. Finally, determination of the analytical model of the CIR with variation in distance and a comparison with the simulated CIR is presented in the latter part of the paper.

2 TESTBED

The physical testbed is shown in Figure 1 while its internal layout is described in Figure 2. This section describes the testbed components and outlines an approach to model it in a particle-based simulator.

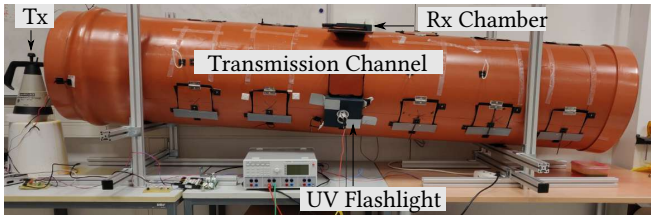

Figure 1: Testbed for air-based molecular communication using fluorescein with a 2 m long transmission channel.

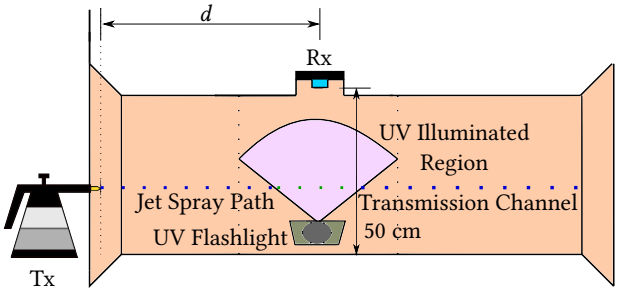

Figure 2: Internal layout of the air-based molecular communication testbed.

2.1 Information Carriers

The Tx is filled with a water-uranine-based solution, where uranine, a disodium salt of fluorescein acts as the information carrier over the transmission channel. Uranine is an amorphous organic compound which produces a peak emission of approximately 548 nm when excited by a UV light source at approximately 390 nm in solution state. The compound is slightly soluble in both water and alcohol. The binary bit "1" is transmitted when the solution is sprayed into the channel under the influence of the UV light source while a bit "0" is transmitted when the solution is not sprayed. This modulation technique is commonly known as on-off keying in the literature.

In the simulation scenario, particles represent these information carriers, which is a commonly-used approach to simulate fluids [13]. Next to their position, they require a spatial description as well to allow for taking overlaps, etc. into account later on. With the help of the particle positions it is possible to represent them as spheres in space. Instead of the handling of light sources and the reflection behavior of the particles, each of the visualized spheres has the same uniform color. So, potential inhomogeneous influences of the light source are ignored. The size of the particles is also set to a constant value.

2.2 Transmitter

The *Gloria Type 89* industrial sprayer is used for spraying the water-uranine-based solution and forms the Tx part of the testbed. The maximum capacity of the container is 1 L while the integrated pump generates a pressure up to 3 bar. The liquid is released outside the container through a conical nozzle in either "cloudy" or "jet"-like spray formation. In this work, we consider the "jet" spray form. At a maximum pressure, the spraying volume rate is around 0.54 L/min. The switching mechanism of the sprayer is electronically controlled

by a 12 V solenoid valve placed before the nozzle. The valve has a maximum tolerance pressure of 10 bar which is controlled by a waveform generator and a control circuit. The minimum shutting time of the valve is 30 ms which influences the shape of the impulse response in the time-domain.

The presented approach to model this nozzle in a particle-based simulator follows a three parameter model which describes the nozzle by the number of injected particles N, their initial velocity v_{Init}, and distribution P in 2-dimensional space corresponding to the opening angle of the nozzle. When spraying towards a sheet of paper vertically as in Figure 3b, the shape approximates a circle. So, it is feasible to start modeling a 2-dimensional model and apply a rotation around the nozzle's spray direction with a uniformly distributed angle $\alpha \sim U_\alpha(0, 2\pi)$ to enable the translation into a 3-dimensional model. It is not possible to measure a clear diameter of the projected circle as it has no hard outline but fades to surrounding sparkles. This motivates using a non-uniform distribution for P for the nozzle model. Each injected particle will have a velocity computed as

$$\begin{pmatrix} v_x \\ v_y \\ v_z \end{pmatrix} = v_{\text{Init}} \cdot \begin{pmatrix} \sin(\beta) \cdot \sin(\alpha) \\ \cos(\beta) \\ \sin(\beta) \cdot \cos(\alpha) \end{pmatrix}, \tag{1}$$

where $\beta \sim P$. This sprays particles into the positive y-direction. Other spray directions can be realized by performing another rotation transformation on the velocity vectors.

In order to calibrate this model to the spray nozzle used in the testbed, the parameters v_{Init} and the distribution P have to be determined. To estimate the velocity v_{Init} and to better understand the spraying process of the nozzle in general, a high-speed camera capturing 1000 frames per second (FPS) provides helpful video footage. A grid paper in the background supports the velocity estimation for the first 30 cm. The image in Figure 3a depicts one frame of this video. As the paper is put behind the nozzle with as little distance as possible between nozzle and paper, perspective offsets can be neglected. The footage outlines a water jet shape which is not affected by air drag as much as a single particle. By tracking the front of the water jet on the grid for each frame, an estimation of the velocity is possible. The water jet speeds up in the first ten frames and reaches a constant velocity for the last frames. Based on ten repetitions of this experiment, the mean velocity is around 12.82 m/s. Because of the image being blurry, the precision for estimating the head position of the water jet is half the distance between two lines (0.25 cm).

To verify that air drag is negligible even for larger distances in the testbed, the camera footage of the previous experiment would not deliver the required precision for tracking the head of the water jet. Instead, the time between transmission and reception for a known distance d is measured. One camera (A) observes the Tx and an additional LED which is put into the frame (A). The Rx, being a camera as well, has another LED within its view (B). This setup is outlined in Figure 4.

All three components, the sprayer and both LEDs, are turned on at the same time. For the Tx video, the number of frames between the LED turning on and the first particles leaving the nozzle denotes the transmission offset Δn_{Tx}. Similarly, on Rx side, the number of

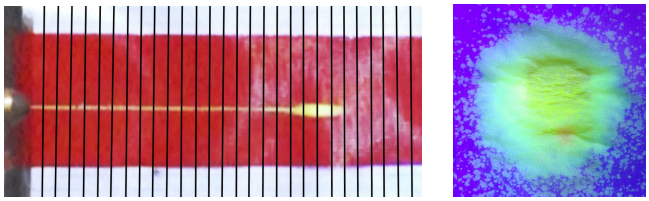

(a) Video footage analysis for estimating the velocity of the particles.

(b) Projection of a spray injection on a paper at 117 cm.

Figure 3: Experiments to obtain a better understanding of the spray nozzle behavior.

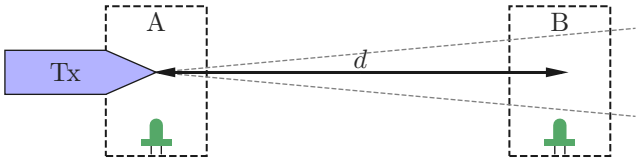

Figure 4: Setup of an experiment to estimate the speed of the particles by utilizing LEDs to measure the time between transmission start and reception at a given distance.

frames between the LED turning on and the first particles hitting the center of the frame denotes the Rx offset Δn_{Rx}. The camera has a frame rate f_{Camera}. Together with the distance d between Tx and Rx the velocity can be computed as

$$v = \frac{d}{(\Delta n_{\text{Rx}} - \Delta n_{\text{Tx}}) \cdot f_{\text{Camera}}}. \tag{2}$$

The obtained velocity of this setup for a distance of 117 cm is 12.77 m/s with an error of around 0.3 m/s due to the frame rate of the used camera (480 FPS). The resulting interval contains the outcome of the previous experiment and therefore confirms the assumption of simulating the testbed particles with a constant velocity. So, the more precise value of 12.82 m/s denotes v_{Init} for the calibrated spray nozzle model.

Another lesson learned from evaluating this video footage is that for larger distances the jet loses its formation and *spreads* or *splits* into several parts with slightly different velocities. The video does not provide enough information for describing these differences in more detail. Nevertheless, to consider this effect in the model, particles should also have slight differences in their initial velocity which can be modeled by using a normal distribution $N(\mu = v_{\text{Init}}, \sigma)$. As there is no experiment to determine σ, variation of this parameter is used to approximate testbed results.

Previous experiments do not give an insight into the spatial distribution of particles. So, in another setup the spray nozzle injects particles for a longer period of time (approx. 1 s) and Rx is placed at different distances. Particles travel through the obtained Rx video—which uses landscape format—from left to right. By taking the central column of the video for each frame and appending it to a new image, it is possible to generate a heat map of the particles at the corresponding row of the video over time. When summing up all values of a row, this heat map reveals the distribution of particles.

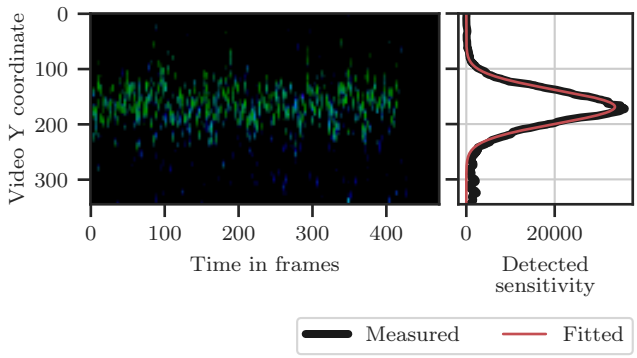

Figure 5: Heat map and distribution of particles from the receiver's perspective at a distance of 88 cm to the injector.

Figure 5 outlines this experiment for a distance of 88 cm. Subtracting the first frame from all others improves the quality as it cancels out constant disturbances like reflections of the light source on the ground. In addition, pixels below a given threshold are marked as black to imitate a noise gate. The curve approximates a normal distribution. So, it becomes possible to replace the distribution P in Equation (1) by $N(\mu, \sigma)$ with $\mu = 0$ as the position of the injector is a separate attribute and an estimated $\sigma = 1.55$ for the given nozzle.

When injecting only a single particle per time step, this can lead to fairly high distances between the individual particles as shown in Figure 6a and does not reflect the expected water jet shape. One possibility to solve this issue is to set the step size of the simulator rather small. However, this in turn leads to a decrease in simulation speed. Hence, the injector is able to inject multiple particles per time step and computes an even offset to one another. As shown in Figure 6b, using the same step size but increasing the number of injected particles will lead to a smaller distance between them when following this approach.

(a) Single injection per time step can lead to a noticeable distance between particles.

(b) Multiple injected particles per time step and an offset to one another decreases the distance between particles.

Figure 6: Distance between particles for the same step size, using a single and multiple injections per time step.

2.3 Transmission Channel

The transmission channel consists of a tube of diameter 50 cm and a length of 2 m which may be extended further by attaching additional tubes. The tube consists of three rows of six opening flaps, each separated from its neighbor by a distance of 30 cm. The detection and the UV light chambers are mounted on these flaps at varying distances from the Tx for detection purposes. The aluminium frame forms the support structure on which the tube rests. The tube could also be tilted at different angles to facilitate proper drainage of the water-based solution out of the tube. Once the flaps are closed, the internal environment of the tube is left completely dark in order to avoid interference from the environmental light.

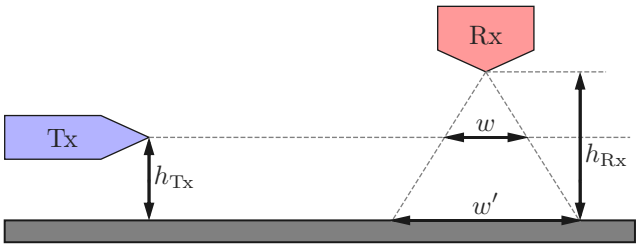

Figure 7: Experiment to estimate the view of the camera.

The simulator moves carriers in discrete time steps. When the Tx injects them into the tube which is filled with air, there are no collisions between the particles and the tube before they reach the view of Rx. So, the channel used for the simulation can be considered unbounded. When the particles move through the air, several effects influence their movement like gravity and air drag. As their initial velocity is relatively high with respect to the distance between Tx and Rx, such effects can be neglected. The new position of each particle $\vec{p}_n$ at time step n is calculated from its previous position $\vec{p}_{n-1}$, its velocity $\vec{v}$, and the step size Δt as

$$\vec{p}_n = \vec{p}_{n-1} + \Delta t \cdot \vec{v}. \tag{3}$$

2.4 Receiver

The Rx constists of a high-speed digital camera capturing the images of the spray droplets passing through the transmission channel at 480 FPS. The region in focus of the camera is illuminated by an 18 W UV flashlight in the range of 390 nm in order to excite the liquid droplets containing the uranine molecules. The post-processing algorithm implemented compensates for the effect of offset by subtracting the first frame from the subsequent frames. The light intensity is then recorded by the camera from the droplets which is normalized to the maximum value over all green pixels. A threshold-based detection can thereby be performed in order to detect the pulses generated for data transmission. It is also worth mentioning that the light intensity can directly be related to the fluorescein concentration [17].

By placing the camera on top of the tube while facing downwards the view of the camera is limited. To estimate the dimensions of this view—its height and width—to be reproduced in the simulation, Figure 7 helps to compute these values. As it is possible to measure h_{Tx} and h_{Rx} as well as w' (by marking and measuring the edges of the view at the bottom of the tube), the intercept theorem allows to calculate the width of the view w. The aspect ratio of the camera enables to calculate the height h based on the width.

One approach to model Rx in a particle-based simulator is a simple *counting sensor* which counts the number of particles within this specific region. However, this would not incorporate the effect of overlapping particles. So, the simulator generates a video from the camera's perspective which depicts the particles. In the same way the post-processing script computes the received signal strength from the video footage of the testbed camera, it is possible to apply this script on the generated footage. This leads to a two step

reception process for simulations: (i) generating a video from Rx perspective and (ii) detecting the signal strength by post-processing this video. As the script for step (ii) is already given, the focus of the simulator lies on the generation of the video. Currently, this video is generated by using the 3D capabilities of Matplotlib.

3 CHANNEL IMPULSE RESPONSE

The detection is performed using a high-speed digital camera. The spray pulses are recorded which are assumed to be Gaussian-shaped in time-domain [4, 8]. Thus, the proposed CIR model is given as

$$h(t) = \frac{a}{b\sqrt{2\pi}} \exp\left(-\frac{(t-t_0)^2}{2b^2}\right), \tag{4}$$

where a is the intensity from the detected droplets with some attenuation factor, b is the spreading of the pulse in time-domain, while t_0 is the center or the mean of the Gaussian pulse. The goal is to determine the variation of coefficients a and b with distance between Tx and Rx for testbed measurements and simulation data.

The parameters used in the experiment are listed in Table 1. For each distance, the measured CIR of the testbed and simulation is averaged over 60 trials. One example of the 60 measured CIRs of the testbed before averaging is shown in Figure 8. Finally, the analytical model is fitted through the averaged CIR over the considered sample points, using the non-linear least squares curve-fitting algorithm.

The average measured impulse responses along with both fitted models are also shown in Figure 8. As it is a challenge to determine the zero time-stamp of the testbed data, synchronizing it with the simulation data is done by aligning the rising edges of the received signals. The maximum value of the simulation data is scaled to match with the maximum value of the testbed. This is necessary since the testbed illumination is inconsistent between distances, which the simulation does not account for.

For a distance of 58 cm, the measured CIR of the testbed data is skewed at the beginning of the peak. When the first droplets are released out of the nozzle, a "blob"-like formation as depicted in Figure 3a forms due to inertia causing a conglomeration of smaller droplets. As the droplets travel farther, the "blob" eventually spreads out and disintegrates into smaller droplets, reducing its effect at higher distances. This blob is not considered in either model, which is expected to cause deviation from the testbed results.

For the rising edge, the simulator tends to approximate the testbed behavior better than the analytical model. However, the rising edge of the simulated data is still less steep compared to the testbed data. A more precise estimation of the initial velocity distribution might improve this mismatch.

Table 1: Simulation parameters used for analysis.

Parameter	Value
Bit duration	0.05 s
Spray duration	0.02 s
Distance to Rx	58, 88, 118, 148, and 178 cm
Spray pressure	3 bar
Spray volume rate	0.54 L/min
Camera frame rate	480 FPS

The testbed signal has an additional tail after the falling edge of the peak, potentially caused by slower particles. This becomes more obvious with increasing distance between Tx and Rx. One reason for this deviation can be air drag, which slows down particles in the testbed. Another issue is the switching process of the spray nozzle, which is not instantaneous as assumed in the spray nozzle model.

Figure 9 shows the change in magnitude of coefficient a with distance. The value decreases almost linearly with growing distances. This is attributed to the fact that there is a reduction in the number of droplets traversing the length of the tube, as some droplets either fall down or get dispersed laterally. This increases the distance between the droplets and the camera for higher distances, resulting in a reduction of the light intensity received by the camera. Some droplets might even collide with the enclosing tube and therefore not reach the detector at all. As currently neither gravity nor the influence of light or tubing are modeled in the simulation, the coefficient a is not calculated for the simulation.

The value of coefficient b increases initially up to 118 cm and decreases afterwards, as shown in Figure 9. This corresponds to a reduced peak width observed in the testbed at higher distances. The parabolic trajectory decreases the distance between droplets and light source, decreasing consequently the duration of particles being illuminated before leaving the light cone again. The camera, therefore, detects only a smaller part of the pulse actually getting illuminated, giving the impression of a CIR with a lower time-domain spread. This problem is worsened by the necessary video de-noise filtering, which might also filter out some less well-illuminated droplets entirely. Together, these effects could account for the difference between simulation and experiment.

4 CONCLUSION

An air-based MC testbed using fluorescein is presented in this work. From CIR analysis, it is concluded that the bit duration of 0.05 s is expected to give a quasi-error-free transmission at 20 bits/s over the testbed channel with low ISI. This is much faster than the existing fluorescence-based MC using water as transmission channel. The measured CIR along with the simulation and analytical models are shown with variation in distance. Higher data rates are expected for sophisticated modulation schemes. Equalization and channel coding schemes are also anticipated to reduce the effect of ISI and noise originating in the testbed. The aforementioned tasks are planned for the future work along with bit error rate analysis. The camera-based detector may also be replaced by a photodetector. The simulation of the testbed with the *Pogona simulator* required the implementation of a new injector and Rx model. The proposed model of a spray nozzle injector requires three parameters: the number of injected particles per time step and their initial velocity distribution (direction and absolute value). Effects like air drag and gravity, influence particle movement and should be incorporated in future work to especially improve the simulation over larger distances where the impact becomes more significant. Additionally, it is now possible to generate a video from a camera Rx that detects illuminated particles from a user-defined perspective. One simplification made is homogeneous lighting of the particles which does not reflect the real world behavior according to video footage taken

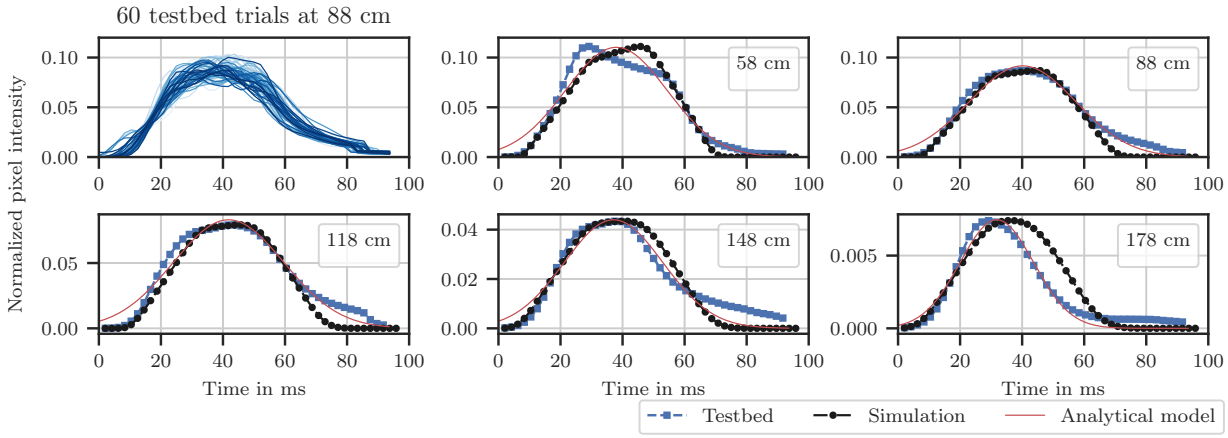

Figure 8: Impulse responses for different distances.

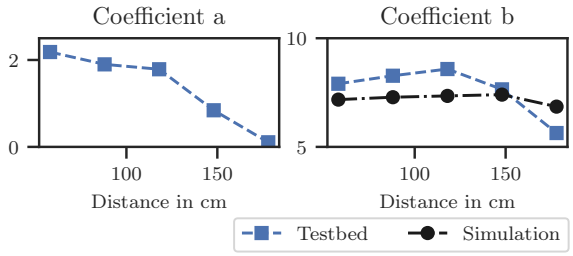

Figure 9: Variation of coefficients a and b with distance.

from the testbed. To improve the quality of the generated video, the influence of light needs to be simulated in future work.

ACKNOWLEDGMENTS

Reported research was supported in part by the project *MAMOKO* funded by the German Federal Ministry of Education and Research (BMBF) under grant numbers 16KIS0915 and 16KIS0917.

REFERENCES

[1] Mahmoud Abbaszadeh, Weiqiu Li, Lin Lin, Iain White, Petr Denissenko, Peter J. Thomas, and Weisi Guo. 2019. Mutual Information and Noise Distributions of Molecular Signals using Laser Induced Fluorescence. In *IEEE Global Communications Conference (GLOBECOM 2019)*. Waikoloa, HI. https://doi.org/10.1109/GLOBECOM38437.2019.9013877

[2] Iresha Atthanayake, Siavash Esfahani, Petr Denissenko, Ian Guymer, Peter J. Thomas, and Weisi Guo. 2018. Experimental Molecular Communications in Obstacle Rich Fluids. In *5th ACM International Conference on Nanoscale Computing and Communication (NANOCOM 2018)*. Reykjavík, Iceland. https://doi.org/10.1145/3233188.3233216

[3] Fabian Bronner and Falko Dressler. 2019. Towards Mastering Complex Particle Movement and Tracking in Molecular Communication Simulation. In *6th ACM International Conference on Nanoscale Computing and Communication (NANOCOM 2019), Poster Session*. ACM, Dublin, Ireland, 36:1–36:2. https://doi.org/10.1145/3345312.3345490

[4] Edward A. Bucher, Robert M. Lerner, and Charles W. Niessen. 1970. Some Experiments on the Propagation of Light Pulses Through Clouds. *Proc. IEEE* 58, 10 (Oct. 1970), 1564–1567. https://doi.org/10.1109/PROC.1970.7980

[5] Nariman Farsad, Weisi Guo, and Andrew W Eckford. 2013. Tabletop Molecular Communication: Text Messages through Chemical Signals. *PLOS ONE* 8, 12 (Dec. 2013), 1–13. https://doi.org/10.1371/journal.pone.0082935

[6] Nariman Farsad, H. Birkan Yilmaz, Andrew Eckford, Chan-Byoung Chae, and Weisi Guo. 2016. A Comprehensive Survey of Recent Advancements in Molecular Communication. *IEEE Communications Surveys and Tutorials* 18, 3 (2016), 1887–1919. https://doi.org/10.1109/COMST.2016.2527741

[7] Luca Felicetti, Mauro Femminella, Gianluca Reali, Paolo Gresele, and Marco Malvestiti. 2013. Simulating an in Vitro Experiment on Nanoscale Communications by using BiNS2. *Elsevier Nano Communication Networks* 4, 4 (Dec. 2013), 172–180. https://doi.org/10.1016/j.nancom.2013.08.003

[8] Robert M. Gagliardi and Sherman Karp. 1995. *Optical Communications* (2 ed.). Wiley.

[9] Stamatios Giannoukos, Alan Marshall, Stephen Taylor, and Jeremy Smith. 2017. Molecular Communication over Gas Stream Channels using Portable Mass Spectrometry. *Journal of The American Society for Mass Spectrometry* 28, 11 (July 2017), 2371–2383. https://doi.org/10.1021/jasms.8b05410

[10] Werner Haselmayr, Andreas Springer, Georg Fischer, Christoph Alexiou, Holger Boche, Peter A. Hoeher, Falko Dressler, and Robert Schober. 2019. Integration of Molecular Communications into Future Generation Wireless Networks. In *1st 6G Wireless Summit*. IEEE, Levi, Finland.

[11] Masaru K. Hojo, Kenichi Ishii, Midori Sakura, Katsushi Yamaguchi, Shuji Shigenobu, and Mamiko Ozaki. 2015. Antennal RNA-sequencing analysis reveals evolutionary aspects of chemosensory proteins in the carpenter ant, Camponotus japonicus. *Scientific Reports (Sci. Rep.)* 5, 13541 (Aug. 2015). https://doi.org/10.1038/srep13541

[12] Yubing Jian, Bhuvana Krishnaswamy, Caitlin M. Austin, A. Ozan Bicen, Jorge E. Perdomo, Sagar C. Patel, Ian F. Akyildiz, Craig R. Forest, and Raghupathy Sivakumar. 2016. nanoNS3: Simulating Bacterial Molecular Communication Based Nanonetworks in Network Simulator 3. In *3rd ACM International Conference on Nanoscale Computing and Communication (NANOCOM 2016)*. ACM, New York City, NY, 17:1–17:7. https://doi.org/10.1145/2967446.2967464

[13] Matthias Müller, David Charypar, and Markus Gross. 2003. Particle-Based Fluid Simulation for Interactive Applications. In *ACM SIGGRAPH/Eurographics Symposium on Computer Animation (SCA 2003)*. Eurographics Association, San Diego, CA, 154–159.

[14] Tadashi Nakano, Andrew W. Eckford, and Tokuko Haraguchi. 2013. *Molecular Communication*. Cambridge University Press.

[15] Adam Noel, Karen C. Cheung, Robert Schober, Dimitrios Makrakis, and Abdelhakim Hafid. 2017. Simulating with AcCoRD: Actor-based Communication via Reaction–Diffusion. *Elsevier Nano Communication Networks* 11 (March 2017), 44–75. https://doi.org/10.1016/j.nancom.2017.02.002

[16] Mustafa Ozmen, Eamonn Kennedy, Jacob Rose, Pratistha Shakya, Jacob K. Rosenstein, and Christopher Rose. 2018. High Speed Chemical Vapor Communication Using Photoionization Detectors. In *IEEE Global Communications Conference (GLOBECOM 2018)*. Abu Dhabi, United Arab Emirates. https://doi.org/10.1109/GLOCOM.2018.8647736

[17] Partha Sarathi, Roi Gurka, Gregory A Kopp, and Paul J Sullivan. 2012. A Calibration Scheme for Quantitative Concentration Measurements using Simultaneous PIV and PLIF. *Experiments in fluids* 52, 1 (Jan. 2012), 247–259.

[18] M. M. Sidahmed, M. D. Taher, and R. B. Brown. 2005. A Virtual Nozzle for Simulation of Spray Generation and Droplet Transport. *Biosystems Engineering* 92, 3 (Nov. 2005), 295–307. https://doi.org/10.1016/j.biosystemseng.2005.07.012

[19] Tatsuya Suda, Michael Moore, Tadashi Nakano, Ryota Egashira, and Akihiro Enomoto. 2005. Exploratory Research on Molecular Communication between Nanomachines. In *Genetic and Evolutionary Computation Conference (GECCO 2005)*. Washington, D.C.